

Article

Tuning the Electronic Properties of Homoleptic Silver(I) bis-BIAN Complexes towards Efficient Electrocatalytic CO₂ Reduction

Dominik Krisch¹, He Sun¹, Kevinjeorjios Pellumbi^{2,3} , Kirill Faust⁴ , Ulf-Peter Apfel^{2,3} 
and Wolfgang Schöfberger^{1,*} 

- ¹ Institute of Organic Chemistry, Johannes Kepler University (JKU), Altenberger Straße 69, 4040 Linz, Austria; dominik.krisch@jku.at (D.K.); he.sun@jku.at (H.S.)
- ² Inorganic Chemistry I—Bioinorganic Chemistry, Ruhr University Bochum, Universitätsstraße 150, 44801 Bochum, Germany; kevinjeorjios.pellumbi@rub.de (K.P.); ulf.apfel@rub.de (U.-P.A.)
- ³ Department of Electrosynthesis, Fraunhofer Institute for Environmental, Energy and Safety Technology UMSICHT, Osterfelder Straße 3, 46047 Oberhausen, Germany
- ⁴ Institute of Catalysis (INCA), Johannes Kepler University (JKU), Altenberger Straße 69, 4040 Linz, Austria; kirill.f Faust@jku.at
- * Correspondence: wolfgang.schoefberger@jku.at

Abstract: We report herein the preparation and characterization of six readily assembled bis-coordinated homoleptic silver(I) *N,N'*-bis(arylimino)acenaphthene (BIAN) complexes of general structure [Ag(I)(BIAN)₂]BF₄ and the influence of the electronic properties of the ligand substitution pattern on their performance in electrochemical CO₂ reduction (CO₂R). All the explored catalysts displayed substantial current enhancements in carbon-dioxide-saturated solvents dependent on the ligated BIAN and no significant concurrent H₂ evolution when utilizing 2% H₂O as a proton source. Additionally, preliminary studies, employing a drop-casted ink of 0.4 mg cm⁻² [Ag(I)(4-OMe-BIAN)₂]BF₄ (**Ag4**) immobilized onto carbon paper gas diffusion electrodes in a flow cell with 1M KHCO₃ aqueous electrolyte, resulted in a propitious Faradaic efficiency of 51% for CO at a current density of 50 mA cm⁻².

Keywords: silver; BIAN ligand; CO₂ reduction; electrocatalysis; gas diffusion electrodes



Citation: Krisch, D.; Sun, H.; Pellumbi, K.; Faust, K.; Apfel, U.-P.; Schöfberger, W. Tuning the Electronic Properties of Homoleptic Silver(I) bis-BIAN Complexes towards Efficient Electrocatalytic CO₂ Reduction. *Catalysts* **2022**, *12*, 545. <https://doi.org/10.3390/catal12050545>

Academic Editor: Ali Seifitokaldani

Received: 21 April 2022

Accepted: 15 May 2022

Published: 17 May 2022

Publisher's Note: MDPI stays neutral with regard to jurisdictional claims in published maps and institutional affiliations.



Copyright: © 2022 by the authors. Licensee MDPI, Basel, Switzerland. This article is an open access article distributed under the terms and conditions of the Creative Commons Attribution (CC BY) license (<https://creativecommons.org/licenses/by/4.0/>).

1. Introduction

For decades, the global community has been facing an environmental crisis, resulting in the need to switch from outdated to new, more efficient, energy sources and a more effective way of tackling rising carbon dioxide emissions. The activation of small molecules, such as H₂O [1–4], O₂ [1,5–7], N₂ [8–10], and CO₂ [11–34], in a cost- and energy-efficient way has become one of the key topics in catalysis research.

The main issue concerning the activation of these molecules is the kinetic barrier that needs to be overcome for the catalyzed reaction to take place [16]. Therefore, there is a research focus on the design of novel ligand systems whose metal complexes can be used for the direct electrocatalytic reduction of CO₂ to valuable chemicals, such as carbon monoxide [18–22], formate [20,23,24], methanol [25–27], ethanol [28,29], methane [18,30], ethylene [28,31–33], and acetate [20,34,35].

While a variety of N-type ligands (e.g., porphyrinoids, bipyridine, salen, pincer ligands, etc.) and their metal complexes have been studied previously, the application of BIAN (*N,N'*-bis(arylimino)acenaphthene) ligated metal complexes for electrochemical conversion of carbon dioxide has been scarce [20]. Hitherto, only one family of BIAN ligated complexes for electrocatalytic CO₂ reduction with Re(I)(Ar-BIAN)(CO)₃Hal (Ar = phenyl, mesityl or 2,6-diisopropyl; Hal = Cl or Br) has been reported [22,36]. Homogenous application in an acetonitrile + 2% H₂O mixture of the most active derivative Re(I)(2,6-diisopropyl-

BIAN)(CO)₃Cl led to the production of CO with a maximum Faradaic efficiency of 24% after 4000 s of electrolysis at -1.85 V vs. NHE [22].

Additionally, only a few reports on silver BIAN complexes have been published in the literature, almost exclusively focusing on their synthesis and characterization with none of the studied compounds being utilized for catalytic applications of any sort [37–39].

The research presented here illustrates the first implementation of molecular silver(I) complexes for electrocatalytic CO₂ reduction. The studied redox-active, homoleptic Ag(I) bis-BIAN coordination compounds were readily prepared in high yields and subsequently characterized through various spectroscopic methods (NMR, UV-vis, IR), X-ray photoelectron spectroscopy (XPS), ESI-HRMS, single-crystal X-ray diffraction and electrochemical studies. The metal complexes were examined homogeneously under argon and CO₂, and, heterogeneously, at a carbon paper gas diffusion electrode. The “non-innocent” nature of the BIAN ligands was reflected in the ability of the auxiliary ligands to participate directly in the catalytic cycle by accepting and donating electrons. All the explored complexes displayed alterations in their cyclic voltammograms under CO₂. Addition of H₂O, a proton source, to the solutions under carbon dioxide exhibited a steep increase in cathodic current when employing the corresponding BIAN-ligated silver(I) complexes. We, furthermore, demonstrated that altering the substituents at the aryl-moieties of the BIAN significantly affected the catalytic current during CO₂ electroreduction. Finally, we established the applicability and stability of heterogenized [Ag(4-OMe-BIAN)₂]BF₄ (**Ag4**) over 1 h of galvanostatic electrolysis on GDEs at current densities up to 200 mA cm⁻² in aqueous 1 M KHCO₃ electrolytes with high selectivity towards CO₂R for the generation of CO.

2. Results and Discussion

2.1. Synthesis and Characterization

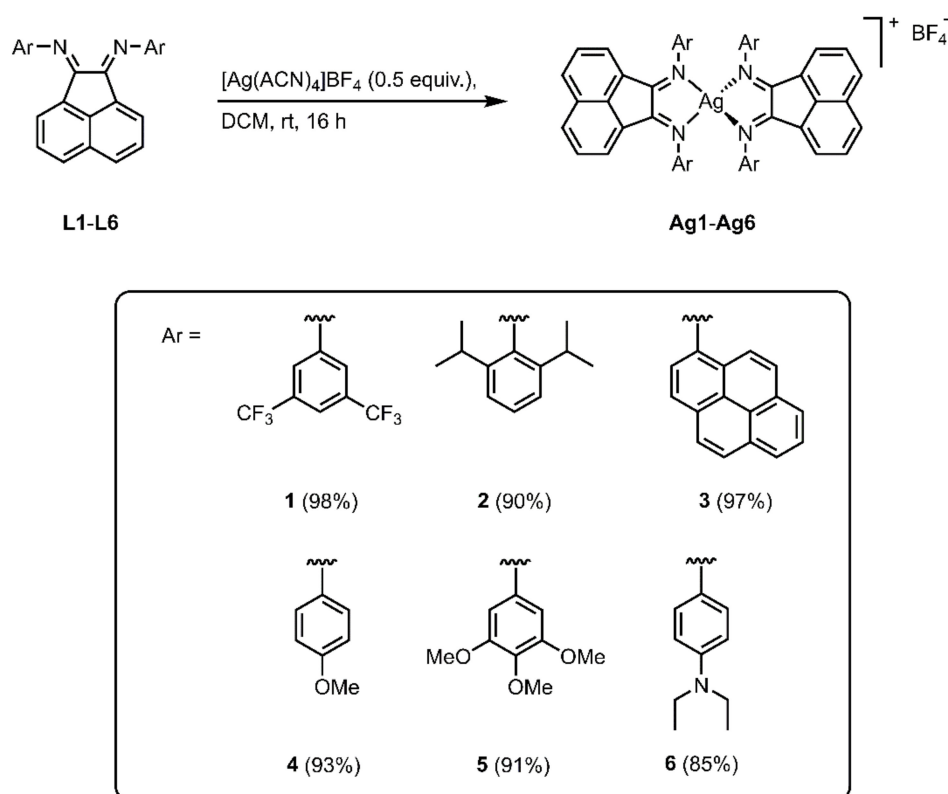
The employed BIAN ligands have been reported before, except for **L3** and **L6**, and were synthesized via the methodologies established by the groups of Ragaini and Milani, with modified workup procedures for **L3**, **L5** and **L6**, as described in the Section 3 (vide infra) [40,41]. In general, stirring acenaphthenequinone and zinc(II) chloride in acetic acid (and toluene for **L1** and **L6**) at elevated temperatures, followed by addition of a slight excess of the respective aniline, led to the formation of BIAN-ligated zinc(II) dichloride precipitate after 15–45 min of reflux. Ensuing demetallation with potassium oxalate resulted in the free BIAN ligands.

The studied homoleptic Ag(I) bis-BIAN complexes were prepared in analogy to a literature procedure, where **Ag2** has been reported [39]. By treating dichloromethane (DCM) solutions of [Ag(I)(ACN)₄]BF₄ (ACN = acetonitrile) with two equivalents of the BIAN ligand, the pertinent bis-chelated [Ag(I)(BIAN)₂]BF₄ complexes **Ag1–Ag6** were isolated in excellent yields of 85–98% (Scheme 1). They were obtained as orange (**Ag1**, **Ag2**), red (**Ag4**, **Ag5**) or purple (**Ag3**, **Ag6**) powders after concentration and subsequent precipitation induced by the addition of *n*-pentane.

Novel BIAN ligands and all silver complexes have been fully characterized by ¹H, ¹³C and ¹⁹F NMR, ESI-HRMS, UV-vis and IR spectroscopy. Due to the multifarious substitution patterns and consequential polarities of the products, however, multiple solvents had to be utilized for these measurements, limiting the direct comparability of some of the obtained data. Solution NMR experiments in CDCl₃, CD₃CN and DMSO-d₆ confirmed that the investigated silver catalysts all exhibited diamagnetic properties, as was to be expected from d¹⁰ metal complexes.

UV-vis spectroscopy revealed that, despite metalation, no intense long-wavelength metal-to-ligand charge-transfer (MLCT) processes occurred in the prepared complexes **Ag1–Ag6** and, predominantly, the intra-ligand centered π - π^* and n - π^* transitions of the aryl, acenaphthene and imine moieties were observed in the acetonitrile solutions [39,42,43]. Nevertheless, these absorptions bands were altered upon coordination to a varying degree, indicating at least some participation of the Ag orbitals with the aforementioned excitations [38]. The UV-vis absorption maxima and corresponding logarithmic extinction

coefficients are listed in Table 1. The most significant alteration of an absorption band was monitored for **L6**, where λ_{\max} of the most bathochromic absorption shifted from 517 nm to 537 nm upon coordination to the silver metal center. In general, the respective lowest energy absorptions were shifted bathochromic in correlation with the increasing electron-donating properties of the BIANs, from 308 (**L1**) up to 517 nm (**L6**), suggesting the energetic convergence of HOMO and LUMO in these systems. The only aberration, with **L3**, can be explained by the incorporation of an extended π -system via the pyrene moiety. This trend also indicated that 4-diethylamino-substituted ligand **L6** was, as would be anticipated, considerably more electron-donating than 4-dimethylamino-BIAN reported in the literature, the equivalent absorption maximum of which is located at 448 nm [44]. The UV-vis spectroscopic data were obtained predominantly with acetonitrile solutions, except for **L3** (DCM), due to its limited solubility and **Ag1**. Measurements of **Ag1** were conducted in tetrahydrofuran (THF), since the highly electron-deficient ligand **L1** has proven to bind weakly to the silver center and is almost instantaneously displaced by rather strongly coordinating solvent molecules, e.g., in ACN.



Scheme 1. Preparation and structures of the evaluated Ag(I) bis-BIAN complexes **Ag1–Ag6**.

Table 1. UV-vis absorption data of the prepared BIAN ligands **L1–L6** and corresponding Ag(I) bis-BIAN complexes **Ag1–Ag6** in acetonitrile (except for **L3** and **Ag1**).

Compound	λ_{\max}/nm (log ϵ)
L1	201 (4.65), 226 (4.71), 297 (3.95), 308 (3.95)
L2	204 (4.99), 229 (4.97), 272 (3.94), 308 (3.93), 409 (2.96)
L3 ^a	245 (5.28), 270 (4.92), 280 (4.97), 348 (4.91), 384 (4.35), 484 (4.04)
L4	212 (4.64), 229 (4.83), 291 (4.08), 424 (3.63)
L5	208 (4.91), 228 (4.94), 300 (3.94), 429 (3.43)
L6	208 (4.82), 229 (4.88), 265 (4.63), 306 (4.27), 317 (4.25), 517 (4.09)
Ag1 ^b	229 (5.35) 297 (4.58)
Ag2	204 (5.20), 229 (5.19), 308 (4.23), 412 (3.30)
Ag3	239 (5.35), 269 (5.02), 279 (5.06), 347 (5.01), 383 (4.45), 474 (4.11)

Table 1. Cont.

Compound	λ_{\max}/nm (log ϵ)
Ag4	212 (4.92), 229 (5.12), 292 (4.36), 422 (3.88)
Ag5	207 (5.12), 228 (5.17), 300 (4.22), 429 (3.72)
Ag6	206 (5.05), 230 (5.09), 268 (4.86), 308 (4.51), 537 (4.38)

^a in DCM. ^b in THF.

The recorded high resolution ESI mass spectra clearly displayed the predicted singly charged cationic complexes missing the non-coordinating BF_4^- anion $[\text{M}-\text{BF}_4^-]^+$.

X-ray quality crystals of **Ag4** were obtained via slow diffusion of *n*-pentane into a dilute DCM solution of the pertinent complex. The derived molecular structure is depicted in Figure 1.

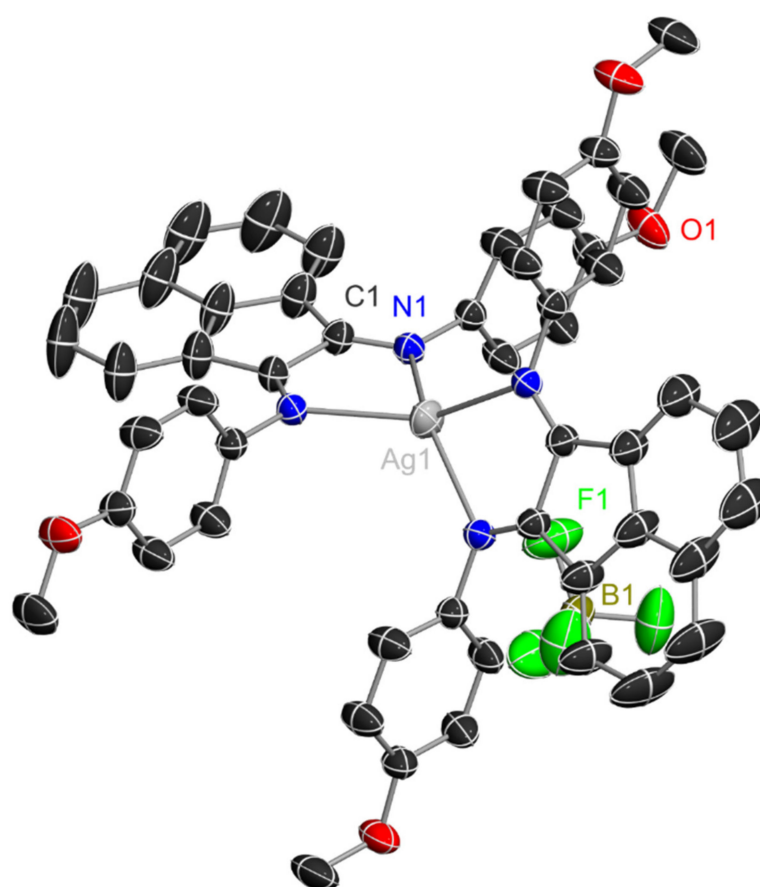


Figure 1. Solid-state molecular structure of Ag(I) bis-BIAN complex **Ag4** in the crystal (*Ccca*). Thermal ellipsoids are drawn at the 30% probability level at 25 °C. Hydrogen atoms are omitted for clarity.

The observed distorted tetrahedral coordination at the Ag(I) metal center in the solid state ($64.040(63)^\circ$ torsion angle between the BIAN planes) was in accordance with the structure published for **Ag2** and was expected to similarly expand onto the other prepared catalysts [39]. All the Ag-N bond lengths of **Ag4** that crystallized in the orthorhombic space group (*Ccca*) were equivalent with 2.327(2) Å. Additionally, this extended to the BIAN C=N and imine C-C bonds with bond lengths of 1.261(4) Å and 1.527(6) Å, respectively. These values were consistent with reported bond lengths of neutral BIAN ligands, further verifying the general structure that was depicted in Scheme 1 [37–39,45–47]. They were nearly identical with the values reported for the molecular structure of the free ligand **L4** [48], illustrating the absence of any particularly strong synergistic interaction from the Ag center to the BIAN, such as extensive π -back bonding, which was in agreement with the data

obtained from UV-vis spectroscopy (vide supra). Furthermore the bite angle of the BIAN at the metal center was determined to be $73.30(11)^\circ$ and the 4-methoxyphenyl moieties were almost perpendicularly ($87.336(104)^\circ$) twisted out of plane of the acenaphthenequinone backbones. Unfortunately, crystals of other Ag complexes could not yet be obtained with sufficient quality or decomposed during the crystallographic measurements.

2.2. Electrochemical Characterization

Cyclic voltammetry for electrochemical characterization and electrocatalytic CO₂ reduction experiments was performed at ambient temperatures and scan rates of 100 mV s⁻¹ with 0.1 M tetrabutylammonium hexafluorophosphate (TBAPF₆) as a supporting electrolyte, typically applying cathodic potentials first. Concentrations of 1 mM catalyst in acetonitrile were studied, except for **Ag2**, where 0.5 mM solutions were examined in consequence of its limited solubility. Additionally, measurements of **Ag1** were conducted in dimethylformamide (DMF) due to the stability limitations elucidated in the previous section. All potentials are given vs. NHE, which were calculated after determination of the ferrocene/ferrocenium half-potential in each mixture as internal standard (listed in Table S2) [49–51].

Cyclic voltammograms (CVs) of the explored complexes under argon were primarily defined by the known distinctive redox non-innocence of BIANs [36,38,43,52–55]. The first reduction generating a radical anion typically delocalized between the imine-moieties occurred between -0.82 (**Ag1**) and -1.32 V (**Ag2**). By further increasing the cathodic potential, a second reduction at the BIAN ligands to the pertinent diamines appeared at -1.06 (**Ag1**) to -1.90 V (**Ag2** and **Ag4**). The data for the electrochemical characterization in anhydrous acetonitrile or DMF under argon is summarized in Table 2.

Table 2. Electrochemical characteristics of catalysts **Ag1–Ag6** compared with **L4**, **L6** and the precursor complex [Ag(ACN)₄]BF₄ at 100 mV s⁻¹ scan rate in ACN under argon. Due to large peak separations, except for the second cathodic reduction, cathodic (pc) and anodic (pa) peak potentials are otherwise given.

Compound	E _{red}			E _{ox}		
	E _{pc} ¹ /V	E _{pa} ¹ /V	E _{1/2} ² /V	E _{pa} ¹ /V	E _{pa} ² /V	E _{pc} ² /V
L4	-1.20	-0.79	-1.78	-	1.25	-
L6	-1.27	-0.94	-1.74	-	0.69	0.64
[Ag(ACN) ₄]BF ₄	-	-	-	0.80	-	-
Ag1 ^a	-0.82	-0.72	-0.99	-	-	-
Ag2	-1.32	-1.08	-1.82	0.67	-	-
Ag3	-0.98	-0.89	-1.83	0.70	1.30	-
Ag4	-1.20	-0.84	-1.82	0.53	1.32	-
Ag5	-1.11	-0.66	-1.76	0.52	1.35	-
Ag6	-1.26	-0.93	-1.73	0.50	0.81	0.71

^a in DMF.

Notably, 4-diethylamino-substituted BIAN **L6** displayed an oxidation reaction that was fully reversible ($E_{1/2} = 0.67$ V), which is extraordinary for this type of α -diimine ligand [38,44,54–56].

The only considerable discrimen of the free BIAN ligands and the respective silver complexes was an oxidation reaction between +0.50 V (**Ag6**) and +0.70 V (**Ag3**), which was not observed for **Ag1** in DMF, with the potentials thereof inversely correlating with the electronic donation of the coordinating ligand. This property was also noted in the electrochemical characterizations of Ag(I) bis-BIAN nitrate complexes that were studied by the Tkachenko group [38]. The oxidative current, however, appeared only if the reductive potentials were applied first, as solely anodic sweeps did not feature in this electrochemical process (see Figure S72). Additionally, this signal was also present in the CV of [Ag(ACN)₄]BF₄ at +0.80 V, but with a many-fold increased current. A CV response

overlay of **L6**, **Ag6** and $[\text{Ag}(\text{ACN})_4]\text{BF}_4$ in acetonitrile under argon is depicted in Figure 2. A tentative explanation would be that some amount of Ag^0 was formed during the cathodic sweeps, which was then re-oxidized upon applying anodic potentials. The substantial decrease in current of this oxidative process for **Ag2–Ag6** indicated the stabilization of the silver(I) metal center within the BIAN-chelated complexes.

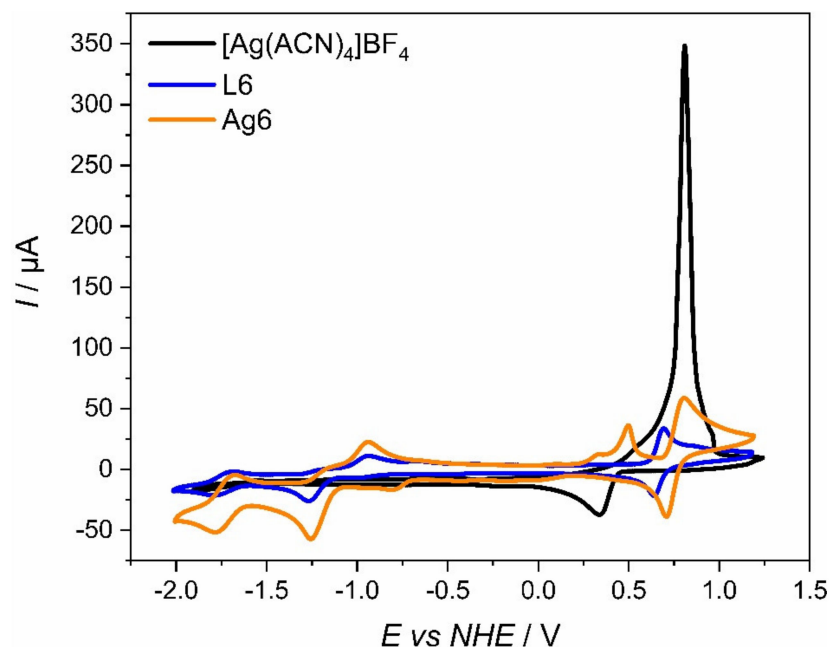


Figure 2. CV response overlay of 1 mM $[\text{Ag}(\text{ACN})_4]\text{BF}_4$, BIAN ligand **L6** and $\text{Ag}(\text{I})$ bis-BIAN complex **Ag6** in ACN under argon at 100 mV s^{-1} scan rate.

2.3. Homogeneous Electrocatalysis

To probe the capabilities of the prepared catalysts **Ag1–Ag6** towards mediating electrocatalytic CO_2 reduction, cyclic voltammograms, employing carbon-dioxide-saturated solvents, with and without the addition of 2 or 20% (for **Ag4** and **Ag6**) of water as a proton source, were recorded, under otherwise identical conditions to those described in the previous section. The introduction of CO_2 into the anhydrous ACN or DMF solutions of the silver catalysts led to an increased cathodic current, except for **Ag3**, typically arising between the first and second ligand-centered reductions. In addition, the transitions became irreversible, confirming a reaction at the electrogenerated species. Although this enhancement for **Ag1–Ag5** was in the range of factors 1.5–3, **Ag6** exhibited a remarkable 15-times higher cathodic current in the presence of CO_2 without a proton source at -1.90 V . The addition of 2% H_2O further augmented the detected reductive currents for **Ag1–Ag5**, however, not when employing **Ag6**, where a slight decrease was noticed, yet still surpassing the other explored catalysts in this study under these conditions. A feasible explanation is that the tertiary *para*-amino functionalities of the BIAN ligand in **Ag6** were protonated to some extent at weakly acidic pH values which were paralleled by CO_2 saturation in the aqueous electrolytes [57]. This alteration resulted in an inversion of the electronic properties of the ligated BIAN, hence becoming electron withdrawing, which as a result partially deactivated the catalyst. The cathodic current densities of **L6** and **Ag1–Ag6** at -1.90 V under the various examined conditions are listed in Table 3.

As depicted in Figure 3 and summarized in Table 3, the catalytic currents in the organic solvent with 2% water mixtures exhibited a positive correlation with increasing electron-donating properties of the employed ligand. Even though the maximum CO_2 concentration at ambient conditions in DMF was lower than in ACN (0.20 M vs. 0.28 M) [58,59], it can clearly be seen that **Ag1**, incorporating the severely electron withdrawing 3,5-bis- CF_3 -BIAN **L1**, produced the lowest cathodic current, despite still exhibiting catalytic activity

(Figure S80). This trend, furthermore, pertained to the onset potentials shifting from ca. -1.65 V (**Ag1**) up to -1.35 V for **Ag6** employing the particularly strongly donating 4-diethylamino-BIAN **L6**.

Table 3. CV current densities (0.28 cm² glassy carbon WE) of 1 mM BIAN ligand **L6** and Ag(I) bis-BIAN complexes **Ag1–Ag6** under argon or CO₂ in anhydrous acetonitrile solutions or with addition of 2% H₂O at a potential of -1.90 V vs. NHE and cathodic scan rate of 100 mV s⁻¹.

Compound	ACN		ACN + 2% H ₂ O	
	$j_{Ar}/\mu\text{A cm}^{-2}$	$j_{CO_2}/\mu\text{A cm}^{-2}$	$j_{Ar}/\mu\text{A cm}^{-2}$	$j_{CO_2}/\mu\text{A cm}^{-2}$
L6	−65	−198	−81	−205
Ag1 ^a	−118	−187	−149	−244
Ag2 ^b	−103	−297	−116	−513
Ag3	−180	−156	−255	−700
Ag4	−177	−354	−187	−895
Ag5	−166	−488	−149	−1263
Ag6	−159	−2264	−158	−2058

^a in DMF. ^b 0.5 mM catalyst solution.

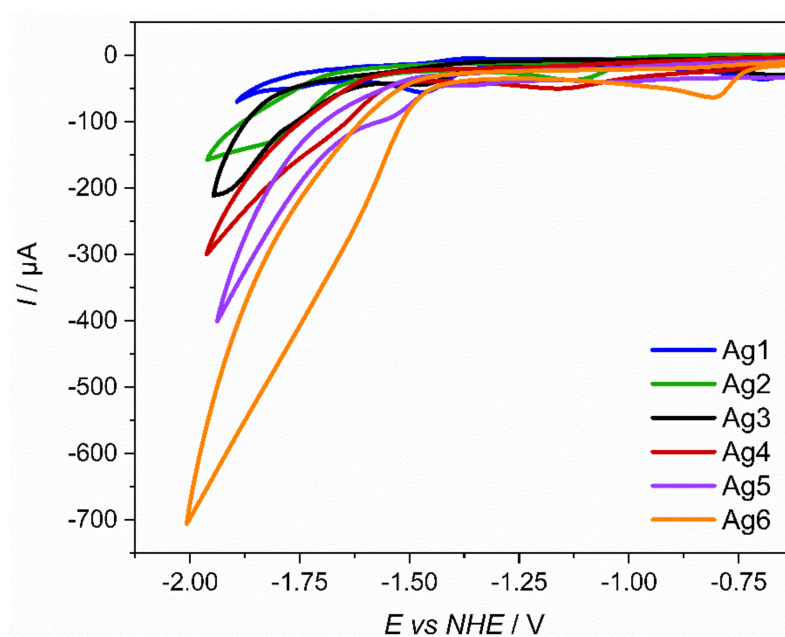


Figure 3. Homogeneous electrocatalysis of Ag(I) bis-BIAN complexes. Cathodic segment of cyclic voltammograms of 1 mM **Ag1–Ag6** (except for 0.5 mM **Ag2**) in CO₂ saturated ACN or DMF (**Ag1**) with 2% H₂O at a scan rate of 100 mV s⁻¹.

The currents observed under anhydrous conditions and in the solvent–water mixtures differed since the presence of protons allowed for alternative reduction mechanisms and, hence, distinct kinetics. It is well known that, without external proton sources, electrocatalytic CO₂ reduction can proceed either via reductive disproportionation forming carbonate and CO, or the more seldom discussed route via dimerization of the radical anion CO₂^{•−} to oxalate, whereas the addition of protons affords varying pathways to a plethora of reduction products, such as CO, formic acid, methanol, methane, and higher carbon products, e.g., ethylene, ethanol and acetic acid [20,29,34,60–63].

Crucial to note is that none of the prepared Ag(I) bis-BIAN complexes displayed notable catalytic H₂ evolution in solvent mixtures with 2% water under argon in the examined potential range. This fact renders them as potent CO₂ reduction catalysts utilizing water as an environmentally benign proton source. CV response overlays of **Ag4** and **Ag6** under different experimental conditions are shown in Figure 4A,C.

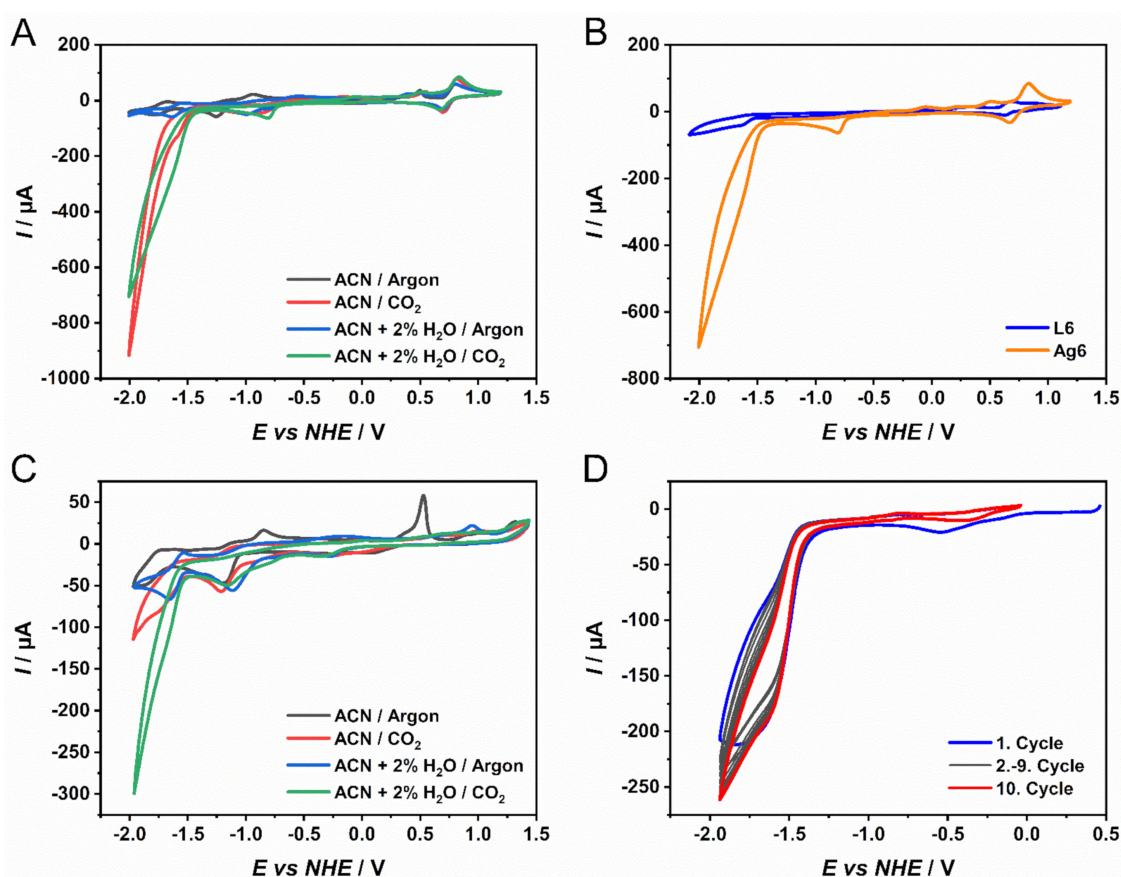


Figure 4. Homogeneous electrocatalysis of BIAN ligand **L6** and Ag(I) bis-BIAN complexes **Ag4** and **Ag6**. (A) Comparison of CVs of **Ag6** in ACN under argon (black), CO₂ (red), in ACN with 2% H₂O under argon (blue) and CO₂ (green) at 100 mV s^{−1} scan rate. (B) CV response overlay of **L6** (blue) and **Ag6** (orange) in ACN with 2% H₂O under CO₂. (C) Comparison of CVs of **Ag4** in ACN under argon (black), CO₂ (red), in ACN with 2% H₂O under argon (blue) and CO₂ (green) at 100 mV s^{−1} scan rate. (D) Stability test of **Ag6** in ACN with 20% H₂O under CO₂ scanning ten purely cathodic cycles not portending a decrease in catalytic current.

Electrochemical studies of the bare BIAN ligand **L6** and the precursor complex [Ag(ACN)₄]BF₄ verified that both the ligand and the coordinated silver metal center were necessary to form catalytically active species, since none of these compounds individually displayed catalytic CO₂ reduction capabilities in ACN/H₂O mixtures comparable to those of the respective chelated silver BIAN complexes (compare Figure 4B and Supplementary Materials). Although the CVs for [Ag(ACN)₄]BF₄ did suggest a considerable increase in cathodic current under CO₂ in the presence of water at potentials below −1.5 V, when scanning over the entire potential region, this current rapidly decreased when the scan range was anodically limited to +0.5 V vs. NHE (Figure S76). This was in contrast to the catalysts **Ag1–Ag6**, which did exhibit stable currents during purely cathodic cycles even with 20% water in ACN (e.g., Figure 4D). This data, in agreement with the heterogeneous CO₂R experiments performed with **Ag4**, clearly indicated that the electrocatalytic CO₂ reduction was mediated by **Ag1–Ag6**, while for [Ag(ACN)₄]BF₄, merely an undefined stoichiometric alteration of the compound, which could be reverted upon oxidation at ca. +0.6 V (in ACN + 20% H₂O), occurred. A similar decrease in the cathodic current was also observed for the BIAN ligand **L6** (Figure S70).

The CVs in ACN + 20% H₂O mixtures for **Ag4** and **Ag6** did exhibit slightly diminished reversibility of the observed redox peaks listed in Table 2, in addition to the ligand-centered reductions arising at less negative potentials (e.g., Figure S94). Nonetheless, electrochemical measurements conducted under an argon atmosphere indicated that no substantial

hydrogen evolution by virtue of water electrolysis was mediated by the explored catalysts, as no significant current increase was observed under these conditions (see, e.g., Figures S91 and S92). The decrease in detected catalytic currents in CO₂ saturated solvents, compared to the experiments conducted with 2% H₂O, was to be anticipated, considering the significantly reduced solubility of CO₂ in water compared to ACN (0.033 M vs. 0.28 M) [58]. It is interesting to note that the catalytic currents of **Ag4** and **Ag6** converged and were nearly identical in ACN with 20% H₂O, further verifying the prior statement regarding the presumed deactivation of **Ag6** induced by chemical alteration of 4-diethylamino-BIAN at weakly acidic pH values, along with the onset potentials of both catalysts being shifted anodic to ca. −1.2 V.

As a final remark, due to the explored catalysts incorporating 18-electron metal centers, it seems counterintuitive, at first, for their catalytic activity to stem from anything other than an outer sphere CO₂ reduction mechanism [20,63–65]. However, solid state molecular structures, inter alia, of five coordinate bis-chelated Ag(I) BIAN nitrate complexes, along with pentaligated [MeB [3-(Mes)pz]₃Ag(C₂H₄)] (Mes = mesitylene; pz = pyrazolate), formally bearing 20 electrons at the metal center, have been reported [38,66]. Hence it appears coherent with this that CO₂ would be able to ligate to the tetracoordinated silver center in the explored compounds **Ag1–Ag6**, generating a reactive intermediate during electrocatalytic reduction.

2.4. Heterogeneous Electrocatalysis

Currently, few materials have achieved a direct transition from homogeneous catalysis to industrially relevant gas diffusion electrodes (GDEs) [19,67]. Concretely, GDEs shorten the diffusion pathways of CO₂ to the catalytic centers compared to H-type cells involving liquid electrolytes, achieving current densities greater than 50 mA cm^{−2} under aqueous conditions [68]. Since **Ag4** has proven pristine catalytic activity and stability towards the generation of CO₂R products when employed homogeneously in high water content solvents, it was selected for preliminary studies on gas diffusion electrodes in a 1 M KHCO₃ electrolyte.

For the fabrication of the GDEs, catalytic inks consisting of a mixture of carbon-black (33 wt.%) and **Ag4**, bound by Nafion, were drop-casted on the surface of an H23C6 carbon paper GDL, at a catalytic loading of 0.4 mg cm^{−2} **Ag4**. Investigation of the pertinent GDEs under 50 mA cm^{−2} to 200 mA cm^{−2} demonstrated that in aqueous electrolytes, **Ag4** still possessed high selectivity towards CO (Figure 5). The constant half-cell potentials (Figure 5B) during galvanostatic electrolysis provided further evidence of the robustness and stability of the explored catalytic system.

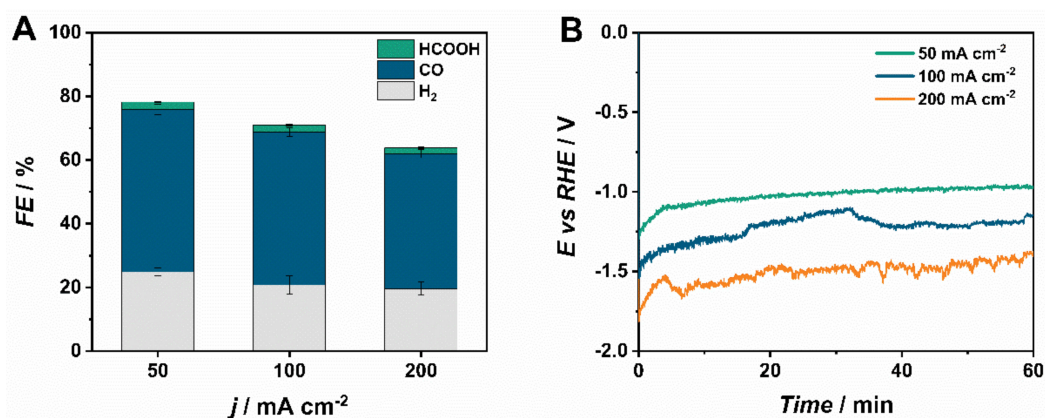


Figure 5. Performance of Ag(I) bis-BIAN complex **Ag4** on H23C6 carbon paper GDL during the heterogeneous electrocatalytic CO₂ reduction process. (A) Faradaic efficiencies after 1 h of galvanostatic electrolysis at different current densities in 1M KHCO₃. (B) Obtained potential curves of galvanostatic electrolysis at different current densities in 1M KHCO₃.

At lower current densities of 50 mA cm⁻² and 100 mA cm⁻², CO was generated with a Faradaic efficiency (FE_{CO}) of 51% and 47%, respectively. Furthermore, regarding industrially relevant current densities of 200 mA cm⁻², **Ag4**-GDEs remained highly active with an FE_{CO} of 42% at half-cell potentials of ca. -1.4 V vs. RHE. The remaining percentages of Faradaic efficiency at higher current densities could have been associated with losses of gaseous products in the catholyte reservoir, underlying the need for improvement regarding the wettability of the electrode surface.

The obtained results clearly demonstrated the promising perspective of Ag-BIAN electrocatalysts towards industrially relevant applications. Previous reports have already shown that optimal CO₂RR activity can be achieved by tailoring, not only the catalyst, but also the reactive environment [69,70], electrode architecture [71] and surrounding parameters [72] in a synergistic fashion. Consequently, our future investigations will focus on optimizing BIAN-coated GDEs in state-of-the-art CO₂ electrolyzers.

3. Materials and Methods

3.1. Synthesis and Characterization

All chemicals were purchased from Alfa Aesar (Kandel, Germany), Strem (Bischheim, France), BLDpharm (Shanghai, China), Merck (Darmstadt, Germany) or Sigma-Aldrich (Vienna, Austria) and were used without further purification unless otherwise noted. Anhydrous DCM, THF and ACN were obtained from a molar sieve MB-SPS-7, M. Braun inert gas-System GmbH (Garching, Germany) under argon atmosphere. All deuterated NMR solvents were purchased from Euriso-Top (Fluorochem, Hadfield, United Kingdom). Proton (¹H NMR), carbon (¹³C NMR) and fluorine (¹⁹F NMR) spectra were recorded on a Bruker (Billerica, MA, USA) DRX 500 MHz spectrometer equipped with a cryoprobe (TXI) and on a Bruker Advance 300 MHz NMR spectrometer. The chemical shifts were given in parts per million (ppm) on the delta scale (δ) and were referenced to the used deuterated solvent for ¹H NMR and ¹³C NMR. High-resolution mass spectra were obtained utilizing an Agilent (Santa Clara, CA, USA) 6520 Q-TOF mass spectrometer with an ESI source and an Agilent G1607A coaxial sprayer. UV-Vis absorption spectra were collected on a Varian CARY 300 Bio spectrophotometer (Agilent, Santa Clara, CA, USA) from 200 to 900 nm. IR spectra were recorded on a Bruker ALPHA II FT-IR instrument. All spectral data can be found in the supporting information.

3.1.1. General Procedure for the Preparation of BIAN Ligands

BIAN ligands **L1**–**L4** and **L6** were synthesized via the methodology established by the Ragaini group with modified workup procedures for **L3** and **L6** as described below [40,41]. In general, acenaphthenequinone and zinc(II) chloride (2.7 equiv.) were stirred in acetic acid (and toluene for **L1** and **L6**) at 80 °C under argon for 30 min. Subsequently, 2.2 equiv. of the respective aniline were added and the mixtures refluxed for 15 (**L2**, **L4**), 30 (**L3**) or 45 min (**L1**, **L6**), leading to the formation of BIAN ligated zinc(II) dichloride precipitate, which was collected via suction filtration. The residues were washed with cold HOAc and Et₂O before being extracted with DCM and saturated aqueous potassium oxalate solution. Finally, the organic layers were dried over Na₂SO₄ and concentrated in vacuo to obtain the free BIAN ligands in yields comparable to the literature.

1-Pyrene-BIAN (**L3**)

According to the literature procedure [40], but with an adapted workup: subsequent to extraction with aq. K₂C₂O₄ and evaporation, the dark residue was triturated with *n*-heptane/ethyl acetate (3:1) thrice to remove residual 1-aminopyrene. The solid was collected via suction filtration, washed with *n*-heptane/ethyl acetate (3:1) and dried in vacuo to obtain 1-pyrene-BIAN **L3** as a dark red-purple powder in 68% yield (2.66 mmol, 1.54 g).

4-Diethylamino-BIAN (L6)

According to the literature procedure [40], but with an adapted workup: subsequent to refluxing the reaction mixture in HOAc/toluene for 45 min, it was cooled in a refrigerator for 1 h. The solution was decanted, and the dark, sticky residue triturated with Et₂O and filtered five times. Afterwards, it was dissolved in MeOH (blue color) and extracted with DCM and saturated aqueous K₂C₂O₄. The now purple organic phase was dried over Na₂SO₄, filtered and concentrated in vacuo to obtain 4-diethylamino-BIAN L6 as a dark purple solid in 66% yield (5.17 mmol, 2.46 g).

3,4,5-Trimethoxy-BIAN (L5)

Synthesized in analogy to a reported procedure [41] with modified workup: 3,5-bis-CF₃-BIAN zinc(II) dichloride complex (1.20 g, 1.58 mmol) was dissolved in 80 mL MeOH, 3,4,5-trimethoxyaniline (868 mg, 4.74 mmol, 3 eq.) added and the solution stirred at rt overnight, during which it turned from orange to red. Subsequently, the reaction mixture was evaporated to dryness, and the residue taken up in DCM and extracted with saturated aqueous K₂C₂O₄ solution. After concentration in vacuo, the oily residue was triturated with *n*-heptane, the remaining solid was dissolved in DCM, extracted five times with 0.1 M HCl and finally washed with water. Afterwards it was dried over Na₂SO₄, filtered and concentrated in vacuo to obtain 3,4,5-trimethoxy-BIAN L5 as a red solid in 66% yield (1.04 mmol, 531 mg).

3.1.2. General Procedure for the Preparation of [Ag(I)(BIAN)₂]BF₄ Complexes Ag1–Ag6

Ag(I) bis-BIAN complexes were prepared analogously to a literature procedure, where Ag2 has been reported [39]. DCM solutions (10 mL) of [Ag(I)(ACN)₄]BF₄ (0.2 mmol) were treated with dropwise addition of BIAN ligand (0.4 mmol, 2 equiv.) in 20 mL DCM, leading to immediate color changes. The resulting mixtures were stirred at room temperature under argon in the dark overnight, before the reaction volumes were reduced to ca. 5 mL under reduced pressure. Subsequently, *n*-pentane was added, the suspensions cooled for 1 h and the precipitated solids collected via suction filtration. After washing the residues with *n*-pentane they were dried in vacuo to obtain Ag1–Ag6 as orange (Ag1, Ag2), red (Ag4, Ag5) or purple (Ag3, Ag6) powders in 85–98% yield (see Scheme 1).

3.2. Homogeneous Electrochemistry

Tetrabutylammonium hexafluorophosphate (TBAPF₆) for the electrochemical measurements was purchased from Sigma-Aldrich and recrystallized twice from absolute ethanol (Acros Organics, Vienna, Austria), dried under high vacuum and stored under argon prior to use. Anhydrous ACN was obtained from a molar sieve MB-SPS-7, M. Braun Inert Gas System GmbH (Garching, Germany) under argon atmosphere. Anhydrous DMF was purchased from Acros Organics. Aqueous solutions for electrochemical experiments were prepared using high purity water (18 MΩ). Homogeneous electrochemical measurements were conducted in a low volume Gamry cell using a three-electrode setup at 25 °C under argon or CO₂, respectively, utilizing a Pine WaveDriver 20 DC Bipotentiostat (Equilabrium, Lyon, France). The investigated solutions were prepared from dry, degassed solvents and contained 0.1 M supporting electrolyte (TBAPF₆) and 1 mM of the respective complexes or ligands, except for [Ag(2,6-dipp-BIAN)₂]BF₄ Ag2, where 0.5 mM solutions were examined in ACN due to its limited solubility. Complex Ag1 was characterized in DMF, since coordinating solvents, such as ACN, cause ligand substitution. For all electrochemical measurements, a glassy carbon (Pine, 65 mm long, 6.4 mm OD PCTFE shroud, 3 mm OD disk) as working electrode, platinum wire (Pine, 65 mm long, 7 mm OD epoxy tube shroud, 0.58 cm² approximate surface area) as counter electrode and a non-aqueous pseudo-Ag/AgCl reference electrode, were used. Prior to each measurement, the glassy carbon WE was polished with a 0.05 μm alumina suspension (deagglomerated, Allied-high tech products) on a MicroCloth polishing pad (Buehler, PSA, Tokyo, Japan). Subsequently, the electrode was cleaned in an ultrasonication bath in pure water for 3 min and finally

rinsed with pure water and acetonitrile to remove any excess of alumina particles. Following each experiment, ferrocene was added as an internal standard. The converted potentials against Fc/Fc^+ were transformed to V vs. NHE with the conversion of +0.630 V vs. NHE in ACN and +0.590 V vs. NHE in DMF according to literature [49–51]. If not otherwise noted, CVs were recorded at a scan rate of 100 mV/s. Plots of the obtained data can be found in the supporting information.

3.3. Heterogeneous Electrochemistry

3.3.1. Fabrication of Gas Diffusion Electrodes

For the catalytic inks, 10 mg of **Ag4** along with 5 mg of Ensaco 250G carbon black (Imerys, Paris, France) were dispersed along with 50 μL of 5 wt.% Nafion 117 solution (Sigma Aldrich, Taufkirchen, Germany) in 5 mL of ethanol. Prior to drop-casting the **Ag4**-containing inks were sonicated for 30 min. Under constant stirring, drop-casting was performed onto the surface of a 22 mm Freudenberg H23C6 GDL (Freundenberg, Weinheim, Germany) placed onto a heated vacuum plate at 80 °C, until a loading of 0.4 mg cm^{-2} of **Ag4** was achieved. The catalytic loading was determined by the mass difference prior to and after drop-casting.

3.3.2. Electrochemical Measurements

The **Ag4**-loaded gas diffusion electrodes were measured in an in-house flow electrolyzer, equipped with parallel titanium flow-fields. Ni-foam (Goodfellow, Hamburg, Germany) was used as the anode, an RHE (Gaskatel, Kassel, Germany) as the reference electrode and an **Ag4**-GDE as the working electrode, with the electrolyte 1M KHCO_3 circulating at a rate of 10 mL min^{-1} . The flow compartment possessed a \varnothing 16 mm opening, thus exposing a 2 cm^2 area of the GDE as the active geometric area with the help of PTFE gaskets.

A CO_2 feed of 22.5 mL min^{-1} was provided to the back-side of the GDE in a flow-by mode, controlled by a mass-flow controller (Bronckhorst, Düsseldorf, Germany). To detect possible changes in the gaseous products streams due to carbonate build-up or due to gas-forming reactions, 10 vol.% Ar (2.5 mL min^{-1}) was added to the CO_2 feed as an internal standard. A differential pressure of 40 mbar was applied with the help of a backpressure regulator (Equilibar, Fletcher, NC, USA). Electrolysis was performed utilizing a Gamry (Haar, Germany) 1010B Potentiostat/Galvanostat for 1 h. All the potential readings were iR-corrected and reported against the RHE. The mean values represented at least three separate measurements, each performed with a new **Ag4**-GDE.

3.3.3. Product Analysis

The composition of gaseous products was determined with the help of an online Shimadzu (Kyoto, Japan) QP2020 GC-MS, equipped with a Supelco Carboxen 1010 Plot column (Sigma Aldrich, Taufkirchen, Germany). Gas samples were taken every 20 min for a total of 1 h. For the quantification of acids, an HPLC 1200 (Agilent, Santa Clara, CA, USA) with a BinPump1200, an autosampler ALS1200 and a DAD detector were used, employing a Phenomenex (Aschaffenburg, Germany) Rezex ROA-Organic Acid H^+ column at a flow rate of 0.2 mL min^{-1} . Before analysis, electrolysis samples were diluted in a 1:5 ratio in 5M H_2SO_4 . Quantification of alcohols was performed with the help of a Shimadzu GCMS-QP2020, equipped with an HS-20 trap system and a SH-Rtx-200MS column.

Calculation of the Faradaic Efficiency

For the gas product quantification, the Faradaic efficiency was calculated as follows:

$$FE = \frac{zF}{i} \cdot x_{prod} \cdot \frac{pF_v}{RT} \cdot 100\% \quad (1)$$

where z is the number of the transferred electrons for the formation of each product, F is the Faraday constant, n_i is the number of moles of the respective product, i is the total applied

current and x_{prod} is the mole fraction of product (x_{meas}) in the gas stream corrected by the internal standard Ar. Moreover, F_v is the initial CO₂ volume flow, p represents the absolute CO₂ pressure, R the gas constant and T the temperature,

$$x_{prod} = x_{meas} \cdot \frac{x_{Ar,input}}{x_{Ar,output}} \quad (2)$$

For liquid products, the following equation was used for the calculation of the FE:

$$FE_i = \frac{z \cdot F \cdot n_i}{i \cdot t} \cdot 100\% \quad (3)$$

where z is the number of the transferred electrons for the formation of each product, F is the Faraday constant, n_i is the number of moles of the respective product, i is the total measured current and t is the time during which the current i was passed through the electrolyte.

4. Conclusions

In summary, we have reported the synthesis and characterization of six homoleptic silver(I) bis-BIAN complexes and assessed their catalytic activity in electrochemical CO₂ reduction. The explored compounds **Ag1–Ag6**, of general structure [Ag(I)(BIAN)₂]BF₄, were readily assembled via two-step syntheses from commercially available starting materials, in good yields, without the prerequisite of dried solvents or manipulations utilizing thorough Schlenk techniques.

Each of the studied complexes **Ag1–Ag6** was shown to mediate the catalytic transformation of carbon dioxide upon the application of cathodic potentials in ACN or DMF and ACN/DMF with 2% H₂O, establishing them as the first described molecular CO₂ reduction catalysts comprising silver metal centers. Juxtaposition of the detected catalytic currents showed that the strongly electron-donating BIANS ameliorated the efficacy of electrochemical CO₂ conversion. Additionally, no significant H₂ evolution was observed for any of the employed catalysts in 2 vol.% aqueous electrolytes under argon at potentials up to -2 V vs. NHE.

Preliminary tests employing 0.4 mg cm⁻² **Ag4**, immobilized with an ink as a heterogeneous catalyst on carbon paper GDEs with 1M KHCO₃ aqueous electrolyte, produced CO at an auspicious 51% FE_{CO} at 50 mA cm⁻² and 42% at 200 mA cm⁻² under as yet non-optimized conditions. These results greatly emphasized the potency of the reported Ag BIAN complexes for electrochemical CO₂ reduction, rendering them particularly appealing for further research and future applications.

Supplementary Materials: The following supporting information can be downloaded at <https://www.mdpi.com/article/10.3390/catal12050545/s1>: The characterization and spectral data of **L1–L6** and **Ag1–Ag6** (¹H NMR, ¹³C NMR, ¹⁹F NMR (for **L1** and **Ag1**), UV-vis, IR, HR-MS, XPS); all homogeneous electrochemical data acquired for **L6**, [Ag(ACN)₄]BF₄ and **Ag1–Ag6**; the description, as well as the results, of the X-ray crystallographic measurements of **Ag4** (CCDC 2167847); and the GC-MS chromatograms of the heterogeneous electrochemistry.

Author Contributions: Conceptualization: D.K. and W.S.; methodology: D.K., H.S., K.P., U.-P.A. and W.S.; validation: D.K., H.S. and U.-P.A.; formal analysis: D.K., H.S., K.P. and K.F.; investigation: D.K., H.S., K.P. and K.F.; writing—original draft preparation: D.K., K.P. and W.S.; writing—review and editing: D.K. and W.S.; visualization: D.K., K.P. and K.F.; supervision: U.-P.A. and W.S.; funding acquisition: U.-P.A. and W.S. All authors have read and agreed to the published version of the manuscript.

Funding: This research was funded by the Austrian Science Fund (FWF Standalone Project P32045), the European Union through the EFRE INTERREG IV ETC-AT-CZ program (project M00146, “RERI-uasb”), the German Federal Ministry for Economic Affairs and Energy (projects “ElkaSyn—Steigerung der Energieeffizienz der elektrokatalytischen Alkoholsynthese”, grant 03ET1642C, and “E4MeWi—Energie-Effiziente Erneuerbare-Energien basierte Methanol-Wirtschaft”, grant 03EI3035A-D), the Deutsche Forschungsgemeinschaft (under Germany’s Excellence Strategy—EXC-2033—Project num-

ber 390677874), and the Fraunhofer Internal Programs under Grant No. Attract 097-602175. Open Access Funding by the Austrian Science Fund (FWF).

Data Availability Statement: Not applicable.

Acknowledgments: We gratefully thank Thomas Bögl from the Department of Analytical Chemistry at the JKU for carrying out ESI HR-MS measurements. W.S. acknowledges the financial support of the Austrian Science Fund (FWF Standalone Project P32045). The NMR spectrometers were acquired in collaboration with the University of South Bohemia (CZ) with financial support from the European Union through the EFRE INTERREG IV ETC-AT-CZ program (project M00146, “RERI-uasb”). K.P. acknowledges the Fonds of the Chemical Industry for a PhD fellowship. U.-P.A. is grateful for financial support from the German Federal Ministry for Economic Affairs and Energy (projects “ElkaSyn—Steigerung der Energieeffizienz der elektrokatalytischen Alkoholsynthese”, grant 03ET1642C, and “E4MeWi—Energie-Effiziente Erneuerbare-Energien basierte Methanol-Wirtschaft”, grant 03EI3035A-D). Furthermore, U.-P.A. is also grateful for the financial support by the Deutsche Forschungsgemeinschaft (under Germany’s Excellence Strategy—EXC-2033—Project number 390677874) and the Fraunhofer Internal Programs under Grant No. Attract 097-602175.

Conflicts of Interest: The authors declare no conflict of interest.

References

1. Lei, H.; Li, X.; Meng, J.; Zheng, H.; Zhang, W.; Cao, R. Structure Effects of Metal Corroles on Energy-Related Small Molecule Activation Reactions. *ACS Catal.* **2019**, *9*, 4320–4344. [[CrossRef](#)]
2. Pan, Y.; Wang, X.; Lu, J.; Yan, Q.; Yuan, W.; Li, C.M. Three-Dimensional Ni Foam-Supported CoO Nanoparticles/N-Doped Carbon Multilayer Nanocomposite Electrode for Oxygen Evolution. *ACS Appl. Nano Mater.* **2020**, *3*, 11416–11425. [[CrossRef](#)]
3. Wang, X.; Fei, Y.; Wang, W.; Yuan, W.; Li, C.M. Polymer-Mediated Self-Assembly of Amorphous Metal–Organic Complexes toward Fabrication of Three-Dimensional Graphene Supported CoP Nanoparticle-Embedded N-Doped Carbon as a Superior Hydrogen Evolution Catalyst. *ACS Appl. Energy Mater.* **2019**, *2*, 8851–8861. [[CrossRef](#)]
4. Yuan, W.; Li, C.; Zhao, M.; Zhang, J.; Li, C.M.; Jiang, S.P. In situ self-assembled 3-D interconnected pristine graphene supported NiO nanosheets as superior catalysts for oxygen evolution. *Electrochim. Acta* **2020**, *342*, 136118. [[CrossRef](#)]
5. Pegis, M.L.; Wise, C.F.; Martin, D.J.; Mayer, J.M. Oxygen Reduction by Homogeneous Molecular Catalysts and Electrocatalysts. *Chem. Rev.* **2018**, *118*, 2340–2391. [[CrossRef](#)] [[PubMed](#)]
6. Miner, E.M.; Fukushima, T.; Sheberla, D.; Sun, L.; Surendranath, Y.; Dincă, M. Electrochemical oxygen reduction catalysed by Ni₃(hexaiminotriphenylene)₂. *Nat. Commun.* **2016**, *7*, 10942. [[CrossRef](#)]
7. Jung, E.; Shin, H.; Hooch Antink, W.; Sung, Y.-E.; Hyeon, T. Recent Advances in Electrochemical Oxygen Reduction to H₂O₂: Catalyst and Cell Design. *ACS Energy Lett.* **2020**, *5*, 1881–1892. [[CrossRef](#)]
8. Foster, S.L.; Bakovic, S.I.P.; Duda, R.D.; Maheshwari, S.; Milton, R.D.; Minteer, S.D.; Janik, M.J.; Renner, J.N.; Greenlee, L.F. Catalysts for nitrogen reduction to ammonia. *Nat. Catal.* **2018**, *1*, 490–500. [[CrossRef](#)]
9. Cui, X.; Tang, C.; Zhang, Q. A Review of Electrocatalytic Reduction of Dinitrogen to Ammonia under Ambient Conditions. *Adv. Energy Mater.* **2018**, *8*, 1800369. [[CrossRef](#)]
10. Qing, G.; Ghazfar, R.; Jackowski, S.T.; Habibzadeh, F.; Ashtiani, M.M.; Chen, C.-P.; Smith, M.R.; Hamann, T.W. Recent Advances and Challenges of Electrocatalytic N₂ Reduction to Ammonia. *Chem. Rev.* **2020**, *120*, 5437–5516. [[CrossRef](#)]
11. Takeda, H.; Cometto, C.; Ishitani, O.; Robert, M. Electrons, Photons, Protons and Earth-Abundant Metal Complexes for Molecular Catalysis of CO₂ Reduction. *ACS Catal.* **2017**, *7*, 70–88. [[CrossRef](#)]
12. Aresta, M.; Dibenedetto, A.; Angelini, A. Catalysis for the valorization of exhaust carbon: From CO₂ to chemicals, materials, and fuels. technological use of CO₂. *Chem. Rev.* **2014**, *114*, 1709–1742. [[CrossRef](#)]
13. Kondratenko, E.V.; Mul, G.; Baltrusaitis, J.; Larrazábal, G.O.; Pérez-Ramírez, J. Status and perspectives of CO₂ conversion into fuels and chemicals by catalytic, photocatalytic and electrocatalytic processes. *Energy Environ. Sci.* **2013**, *6*, 3112. [[CrossRef](#)]
14. Qiao, J.; Liu, Y.; Hong, F.; Zhang, J. A review of catalysts for the electroreduction of carbon dioxide to produce low-carbon fuels. *Chem. Soc. Rev.* **2014**, *43*, 631–675. [[CrossRef](#)]
15. Dedić, D.; Dorniak, A.; Rinner, U.; Schöffberger, W. Recent Progress in (Photo-)Electrochemical Conversion of CO₂ With Metal Porphyrinoid-Systems. *Front. Chem.* **2021**, *9*, 685619. [[CrossRef](#)]
16. Álvarez, A.; Borges, M.; Corral-Pérez, J.J.; Olcina, J.G.; Hu, L.; Cornu, D.; Huang, R.; Stoian, D.; Urakawa, A. CO₂ Activation over Catalytic Surfaces. *ChemPhysChem* **2017**, *18*, 3135–3141. [[CrossRef](#)]
17. Kinzel, N.W.; Demirbas, D.; Bill, E.; Weyhermüller, T.; Werlé, C.; Kaeffer, N.; Leitner, W. Systematic Variation of 3d Metal Centers in a Redox-Innocent Ligand Environment: Structures, Electrochemical Properties, and Carbon Dioxide Activation. *Inorg. Chem.* **2021**, *60*, 19062–19078. [[CrossRef](#)]
18. Shen, J.; Kortlever, R.; Kas, R.; Birdja, Y.Y.; Diaz-Morales, O.; Kwon, Y.; Ledezma-Yanez, I.; Schouten, K.J.P.; Mul, G.; Koper, M.T.M. Electrocatalytic reduction of carbon dioxide to carbon monoxide and methane at an immobilized cobalt protoporphyrin. *Nat. Commun.* **2015**, *6*, 8177. [[CrossRef](#)]

19. Ren, S.; Joulié, D.; Salvatore, D.; Torbensen, K.; Wang, M.; Robert, M.; Berlinguette, C.P. Molecular electrocatalysts can mediate fast, selective CO₂ reduction in a flow cell. *Science* **2019**, *365*, 367–369. [[CrossRef](#)]
20. Kinzel, N.W.; Werlé, C.; Leitner, W. Transition Metal Complexes as Catalysts for the Electroconversion of CO₂: An Organometallic Perspective. *Angew. Chem. Int. Ed.* **2021**, *60*, 11628–11686. [[CrossRef](#)]
21. Zhong, H.; Ghorbani-Asl, M.; Ly, K.H.; Zhang, J.; Ge, J.; Wang, M.; Liao, Z.; Makarov, D.; Zschech, E.; Brunner, E.; et al. Synergistic electroreduction of carbon dioxide to carbon monoxide on bimetallic layered conjugated metal-organic frameworks. *Nat. Commun.* **2020**, *11*, 1409. [[CrossRef](#)] [[PubMed](#)]
22. Portenkirchner, E.; Kianfar, E.; Sariciftci, N.S.; Knör, G. Two-electron carbon dioxide reduction catalyzed by rhenium(I) bis(imino)acenaphthene carbonyl complexes. *ChemSusChem* **2014**, *7*, 1347–1351. [[CrossRef](#)]
23. Dey, S.; Todorova, T.K.; Fontecave, M.; Mougél, V. Electroreduction of CO₂ to Formate with Low Overpotential using Cobalt Pyridine Thiolate Complexes. *Angew. Chem. Int. Ed.* **2020**, *59*, 15726–15733. [[CrossRef](#)] [[PubMed](#)]
24. Kopljar, D.; Inan, A.; Vindayer, P.; Wagner, N.; Klemm, E. Electrochemical reduction of CO₂ to formate at high current density using gas diffusion electrodes. *J. Appl. Electrochem.* **2014**, *44*, 1107–1116. [[CrossRef](#)]
25. Albo, J.; Alvarez-Guerra, M.; Castaño, P.; Irbaien, A. Towards the electrochemical conversion of carbon dioxide into methanol. *Green Chem.* **2015**, *17*, 2304–2324. [[CrossRef](#)]
26. Yang, D.; Zhu, Q.; Chen, C.; Liu, H.; Liu, Z.; Zhao, Z.; Zhang, X.; Liu, S.; Han, B. Selective electroreduction of carbon dioxide to methanol on copper selenide nanocatalysts. *Nat. Commun.* **2019**, *10*, 677. [[CrossRef](#)]
27. Wu, Y.; Jiang, Z.; Lu, X.; Liang, Y.; Wang, H. Domino electroreduction of CO₂ to methanol on a molecular catalyst. *Nature* **2019**, *575*, 639–642. [[CrossRef](#)]
28. Ma, W.; Xie, S.; Liu, T.; Fan, Q.; Ye, J.; Sun, F.; Jiang, Z.; Zhang, Q.; Cheng, J.; Wang, Y. Electrocatalytic reduction of CO₂ to ethylene and ethanol through hydrogen-assisted C–C coupling over fluorine-modified copper. *Nat. Catal.* **2020**, *3*, 478–487. [[CrossRef](#)]
29. Gonglach, S.; Paul, S.; Haas, M.; Pillwein, F.; Sreejith, S.S.; Barman, S.; De, R.; Müllegger, S.; Gerschel, P.; Apfel, U.-P.; et al. Molecular cobalt corrole complex for the heterogeneous electrocatalytic reduction of carbon dioxide. *Nat. Commun.* **2019**, *10*, 3864. [[CrossRef](#)]
30. Pan, H.; Barile, C.J. Electrochemical CO₂ reduction to methane with remarkably high Faradaic efficiency in the presence of a proton permeable membrane. *Energy Environ. Sci.* **2020**, *13*, 3567–3578. [[CrossRef](#)]
31. Chen, Y.; Fan, Z.; Wang, J.; Ling, C.; Niu, W.; Huang, Z.; Liu, G.; Chen, B.; Lai, Z.; Liu, X.; et al. Ethylene Selectivity in Electrocatalytic CO₂ Reduction on Cu Nanomaterials: A Crystal Phase-Dependent Study. *J. Am. Chem. Soc.* **2020**, *142*, 12760–12766. [[CrossRef](#)]
32. Liu, W.; Zhai, P.; Li, A.; Wei, B.; Si, K.; Wei, Y.; Wang, X.; Zhu, G.; Chen, Q.; Gu, X.; et al. Electrochemical CO₂ reduction to ethylene by ultrathin CuO nanoplate arrays. *Nat. Commun.* **2022**, *13*, 1877. [[CrossRef](#)]
33. Ogura, K. Electrochemical reduction of carbon dioxide to ethylene: Mechanistic approach. *J. CO₂ Util.* **2013**, *1*, 43–49. [[CrossRef](#)]
34. De, R.; Gonglach, S.; Paul, S.; Haas, M.; Sreejith, S.S.; Gerschel, P.; Apfel, U.-P.; Vuong, T.H.; Rabeah, J.; Roy, S.; et al. Electrocatalytic Reduction of CO₂ to Acetic Acid by a Molecular Manganese Corrole Complex. *Angew. Chem. Int. Ed.* **2020**, *59*, 10527–10534. [[CrossRef](#)]
35. Liu, Y.; Chen, S.; Quan, X.; Yu, H. Efficient Electrochemical Reduction of Carbon Dioxide to Acetate on Nitrogen-Doped Nanodiamond. *J. Am. Chem. Soc.* **2015**, *137*, 11631–11636. [[CrossRef](#)]
36. Abramov, P.A.; Dmitriev, A.A.; Kholin, K.V.; Gritsan, N.P.; Kadirov, M.K.; Gushchin, A.L.; Sokolov, M.N. Mechanistic study of the [(dpp-bian)Re(CO)₃Br] electrochemical reduction using in situ EPR spectroscopy and computational chemistry. *Electrochim. Acta* **2018**, *270*, 526–534. [[CrossRef](#)]
37. Chen, S.; Huang, Y.; Fang, X.; Li, H.; Zhang, Z.; Hor, T.S.A.; Weng, Z. Aryl-BIAN-ligated silver(I) trifluoromethoxide complex. *Dalton Trans.* **2015**, *44*, 19682–19686. [[CrossRef](#)]
38. Papanikolaou, P.A.; Gdaniec, M.; Wicher, B.; Akivros, P.D.; Tkachenko, N.V. Bis(aryl)acenaphthenequinonediimine Substituent Effect on the Properties and Coordination Environment of Ligands and Their Bis-Chelate Ag^I Complexes. *Eur. J. Inorg. Chem.* **2013**, *2013*, 5196–5205. [[CrossRef](#)]
39. Rosa, V.; Santos, C.I.M.; Welter, R.; Aullón, G.; Lodeiro, C.; Avilés, T. Comparison of the structure and stability of new α-diimine complexes of copper(I) and silver(I): Density functional theory versus experimental. *Inorg. Chem.* **2010**, *49*, 8699–8708. [[CrossRef](#)]
40. Gasperini, M.; Ragaini, F.; Cenini, S. Synthesis of Ar-BIAN Ligands (Ar-BIAN = Bis(aryl)acenaphthenequinonediimine) Having Strong Electron-Withdrawing Substituents on the Aryl Rings and Their Relative Coordination Strength toward Palladium(0) and -(II) Complexes. *Organometallics* **2002**, *21*, 2950–2957. [[CrossRef](#)]
41. Scarel, A.; Axet, M.R.; Amoroso, F.; Ragaini, F.; Elsevier, C.J.; Holuigue, A.; Carfagna, C.; Mosca, L.; Milani, B. Subtle Balance of Steric and Electronic Effects for the Synthesis of Atactic Polyketones Catalyzed by Pd Complexes with Meta-Substituted Aryl-BIAN Ligands. *Organometallics* **2008**, *27*, 1486–1494. [[CrossRef](#)]
42. Rosa, V.; Avilés, T.; Aullón, G.; Covelo, B.; Lodeiro, C. A new bis(1-naphthylimino)acenaphthene compound and its Pd(II) and Zn(II) complexes: Synthesis, characterization, solid-state structures and density functional theory studies on the syn and anti isomers. *Inorg. Chem.* **2008**, *47*, 7734–7744. [[CrossRef](#)] [[PubMed](#)]
43. Löw, I.; Bubrin, M.; Paretzki, A.; Fiedler, J.; Zális, S.; Kaim, W. The BIAN ligand 1,2-bis[(2,6-diisopropylphenyl)imino]acenaphthene: An electron sponge or a “normal” α-diimine ligand? *Inorg. Chim. Acta* **2017**, *455*, 540–548. [[CrossRef](#)]

44. Hasan, K.; Zysman-Colman, E. Synthesis, UV-Vis and CV properties of a structurally related series of bis(Arylimino)acenaphthenes (Ar-BIANs). *J. Phys. Org. Chem.* **2013**, *26*, 274–279. [[CrossRef](#)]
45. El-Ayaan, U.; Murata, F.; El-Derby, S.; Fukuda, Y. Synthesis, structural and solvent influence studies on solvatochromic mixed-ligand copper(II) complexes with the rigid nitrogen ligand: Bis[N-(2,4,6-trimethylphenyl)imino]acenaphthene. *J. Mol. Struct.* **2004**, *692*, 209–216. [[CrossRef](#)]
46. Kern, T.; Monkowius, U.; Zabel, M.; Knör, G. Synthesis, crystal structure and charge transfer spectra of dinuclear copper(I) complexes bearing 1,2-bis(arylimino)acenaphthene acceptor ligands. *Inorg. Chim. Acta* **2011**, *374*, 632–636. [[CrossRef](#)]
47. El-Ayaan, U.; Paulovicova, A.; Fukuda, Y. Structural studies of mixed-ligands copper(II) and copper(I) complexes with the rigid nitrogen ligand: Bis[N-(2,6-diisopropylphenyl)imino]acenaphthene. *J. Mol. Struct.* **2003**, *645*, 205–212. [[CrossRef](#)]
48. Coventry, D.N.; Batsanov, A.S.; Goeta, A.E.; Howard, J.A.; Marder, T.B. Synthesis and molecular structures of α -diimines and their zinc and palladium dichloride complexes. *Polyhedron* **2004**, *23*, 2789–2795. [[CrossRef](#)]
49. Aranzaes, J.R.; Daniel, M.-C.; Astruc, D. Metallocenes as references for the determination of redox potentials by cyclic voltammetry—Permethylated iron and cobalt sandwich complexes, inhibition by polyamine dendrimers, and the role of hydroxy-containing ferrocenes. *Can. J. Chem.* **2006**, *84*, 288–299. [[CrossRef](#)]
50. Pavlishchuk, V.V.; Addison, A.W. Conversion constants for redox potentials measured versus different reference electrodes in acetonitrile solutions at 25 °C. *Inorg. Chim. Acta* **2000**, *298*, 97–102. [[CrossRef](#)]
51. Tsierekzos, N.G. Cyclic Voltammetric Studies of Ferrocene in Nonaqueous Solvents in the Temperature Range from 248.15 to 298.15 K. *J. Solut. Chem.* **2007**, *36*, 289–302. [[CrossRef](#)]
52. Fedushkin, I.L.; Skatova, A.A.; Chudakova, V.A.; Fukin, G.K. Four-step reduction of dpp-bian with sodium metal: Crystal structures of the sodium salts of the mono-, di-, tri- and tetraanions of dpp-bian. *Angew. Chem. Int. Ed.* **2003**, *42*, 3294–3298. [[CrossRef](#)]
53. Hill, N.J.; Vargas-Baca, I.; Cowley, A.H. Recent developments in the coordination chemistry of bis(imino)acenaphthene (BIAN) ligands with s- and p-block elements. *Dalton Trans.* **2009**, 240–253. [[CrossRef](#)]
54. Li, L.; Lopes, P.S.; Rosa, V.; Figueira, C.A.; Lemos, M.A.N.D.A.; Duarte, M.T.; Avilés, T.; Gomes, P.T. Synthesis and structural characterisation of (aryl-BIAN)copper(I) complexes and their application as catalysts for the cycloaddition of azides and alkynes. *Dalton Trans.* **2012**, *41*, 5144–5154. [[CrossRef](#)]
55. Papanikolaou, P.; Akriivos, P.D.; Czapiak, A.; Wicher, B.; Gdaniec, M.; Tkachenko, N. Homoleptic Bis(aryl)acenaphthenequinonediiimine-Cu^I Complexes—Synthesis and Characterization of a Family of Compounds with Improved Light-Gathering Characteristics. *Eur. J. Inorg. Chem.* **2013**, *2013*, 2418–2431. [[CrossRef](#)]
56. Yambulatov, D.S.; Nikolaevskii, S.A.; Kiskin, M.A.; Magdesieva, T.V.; Levitskiy, O.A.; Korchagin, D.V.; Efimov, N.N.; Vasil'ev, P.N.; Goloveshkin, A.S.; Sidorov, A.A.; et al. Complexes of Cobalt(II) Iodide with Pyridine and Redox Active 1,2-Bis(arylimino)acenaphthene: Synthesis, Structure, Electrochemical, and Single Ion Magnet Properties. *Molecules* **2020**, *25*, 2054. [[CrossRef](#)]
57. Gohar, G.A.; Habeeb, M.M. Proton transfer equilibria, temperature and substituent effects on hydrogen bonded complexes between chloranilic acid and anilines. *Spectroscopy* **2000**, *14*, 99–107. [[CrossRef](#)]
58. Jitaru, M. Electrochemical carbon dioxide reduction—Fundamental and applied topics. *J. Chem. Technol. Metall.* **2007**, *42*, 333–344.
59. Gennaro, A.; Isee, A.A.; Vianello, E. Solubility and electrochemical determination of CO₂ in some dipolar aprotic solvents. *J. Electroanal. Chem.* **1990**, *289*, 203–215. [[CrossRef](#)]
60. Kaiser, U.; Heitz, E. Zum Mechanismus der elektrochemischen Dimerisierung von CO₂ zu Oxalsäure. *Ber. Bunsenges. Phys. Chem.* **1973**, *77*, 818–823. [[CrossRef](#)]
61. König, M.; Vaes, J.; Klemm, E.; Pant, D. Solvents and Supporting Electrolytes in the Electrocatalytic Reduction of CO₂. *iScience* **2019**, *19*, 135–160. [[CrossRef](#)]
62. Sullivan, B.P. *Electrochemical and Electrocatalytic Reactions of Carbon Dioxide*; Elsevier Science: Burlington, ON, Canada, 1992; ISBN 9780444596611.
63. Costentin, C.; Robert, M.; Savéant, J.-M. Catalysis of the electrochemical reduction of carbon dioxide. *Chem. Soc. Rev.* **2013**, *42*, 2423–2436. [[CrossRef](#)]
64. Rosokha, S.V.; Kochi, J.K. Continuum of outer- and inner-sphere mechanisms for organic electron transfer. Steric modulation of the precursor complex in paramagnetic (ion-radical) self-exchanges. *J. Am. Chem. Soc.* **2007**, *129*, 3683–3697. [[CrossRef](#)] [[PubMed](#)]
65. Savéant, J.-M. Molecular catalysis of electrochemical reactions. Mechanistic aspects. *Chem. Rev.* **2008**, *108*, 2348–2378. [[CrossRef](#)] [[PubMed](#)]
66. Dias, H.V.R.; Fianchini, M. A classical silver carbonyl complex {MeB[3-(Mes)pz]₃}Ag(CO) and the related silver ethylene adduct {MeB[3-(Mes)pz]₃}Ag(C₂H₄). *Angew. Chem. Int. Ed.* **2007**, *46*, 2188–2191. [[CrossRef](#)]
67. Wan, Q.; He, Q.; Zhang, Y.; Zhang, L.; Li, J.; Hou, J.; Zhuang, X.; Ke, C.; Zhang, J. Boosting the faradaic efficiency for carbon dioxide to monoxide on a phthalocyanine cobalt based gas diffusion electrode to higher than 99% via microstructure regulation of catalyst layer. *Electrochim. Acta* **2021**, *392*, 139023. [[CrossRef](#)]
68. Jaster, T.; Gawel, A.; Siegmund, D.; Holzmann, J.; Lohmann, H.; Klemm, E.; Apfel, U.-P. Electrochemical CO₂ reduction toward multicarbon alcohols—The microscopic world of catalysts & process conditions. *iScience* **2022**, *25*, 104010. [[CrossRef](#)] [[PubMed](#)]
69. Pellumbi, K.; Smialkowski, M.; Siegmund, D.; Apfel, U.-P. Enhancing the CO₂ Electroreduction of Fe/Ni-Pentlandite Catalysts by S/Se Exchange. *Chemistry* **2020**, *26*, 9938–9944. [[CrossRef](#)] [[PubMed](#)]

70. Tetzlaff, D.; Pellumbi, K.; Puring, K.j.; Siegmund, D.; Polet, W.S.K.; Checinski, M.P.; Apfel, U.-P. Influence of the Fe: Ni Ratio in $\text{Fe}_x\text{Ni}_{9-x}\text{S}_8$ ($x = 3-6$) on the CO_2 Electroreduction. *ChemElectroChem* **2021**, *8*, 3161–3167. [[CrossRef](#)]
71. Junge Puring, K.; Siegmund, D.; Timm, J.; Möllenbruck, F.; Schemme, S.; Marschall, R.; Apfel, U.-P. Electrochemical CO_2 Reduction: Tailoring Catalyst Layers in Gas Diffusion Electrodes. *Adv. Sustain. Syst.* **2021**, *5*, 2000088. [[CrossRef](#)]
72. Hoof, L.; Thissen, N.; Pellumbi, K.; Junge Puring, K.; Siegmund, D.; Mechler, A.K.; Apfel, U.-P. Hidden parameters for electrochemical carbon dioxide reduction in zero-gap electrolyzers. *Cell Rep. Phys. Sci.* **2022**, *3*, 100825. [[CrossRef](#)]